Tellus (1995), 47A, 911–919
Printed in Belgium – all rights reserved

TELLUS
ISSN 0280–6495

On the nature of the mesoscale circulations at a kata-cold front

By K. A. BROWNING, *Joint Centre for Mesoscale Meteorology, Harry Pitt Building, University of Reading, Whiteknights Road, PO Box 240, Reading RG6 6FN, UK*

(Manuscript received 16 September 1994; in final form 14 November 1994)

ABSTRACT

A series of dropwindsondes released over the sea during the FRONTS 92 experiment is analysed to reveal the mesoscale structure of a kata-cold front characterised broadly by a dry airstream over-running a warm moist boundary layer. The front had a multiple structure with two main surface fronts and this paper is concerned with the detailed structure of one of the surface cold fronts. Two kinds of circulations are shown to coexist at such a front: vertical convection and a slantwise circulation. The slantwise circulation is a feature not normally resolved by conventional observations of kata-cold fronts: it is shown to be a small-scale version of the rearward-sloping ascent encountered in ana-cold fronts. Much of the slantwise circulation was cloud-free but where it impinged upon the boundary layer it triggered the development of a narrow band of convective cloud, the tops of which extended downstream within air that was overtaking the front.

1. Introduction

The two main classes of cold front were classified by Bergeron (1937) and Sansom (1951) as either ana-fronts or kata-fronts according to whether ascending or descending airflows dominate their structure. Ana-cold fronts are characterised by rearward-sloping ascent of air with high wet-bulb potential temperature (θ_w). Much of this warm air originates as a strong low-level flow just ahead of the surface cold front. The warm air ascends above the advancing wedge of cold air. In NW Europe, however, such fronts are rather less common than kata-cold fronts.

Kata-cold fronts are superficially quite different: in kata-cold frontal situations, the warm air (see shaded arrow labelled Warm Conveyor Belt in Fig. 1) ascends in advance of the cold front and is overrun by dry, low-θ_w air (unshaded arrow in Fig. 1). This overrunning airstream originates in the upper troposphere or lower stratosphere and is known as the dry intrusion. The leading edge of the dry intrusion constitutes an upper cold front or moisture front. Because of this separation between the surface cold front (SCF) and upper cold front (UCF), the combined system is referred to as a split front (Browning and Monk, 1982). The surface cold front in a split-front system is what is referred to by Sansom as a katafront.

A feature of kata-cold fronts, glossed over in the simple split front model, is the fine structure that occurs within the SCF part of the split front. As seen in satellite imagery, this often manifests itself as multiple, rather shallow and narrow, cloud bands. Each band corresponds to a slight local sharpening of the generally rather diffuse low-level cold frontal zone that characterises most kata-cold fronts. In this paper we present some exceptionally detailed observations of such a multiply-banded SCF. There were two main cold frontal bands in this case and we concentrate on just one of them so as to derive a conceptual model of the dynamic and thermodynamic structure of an individual SCF. A feature of the model is that two distinct kinds of circulation can coexist in association with a single SCF cloud band: (i) a small-scale slantwise circulation; (ii) vertical convective cells.

In some respects, the structure resembles that of

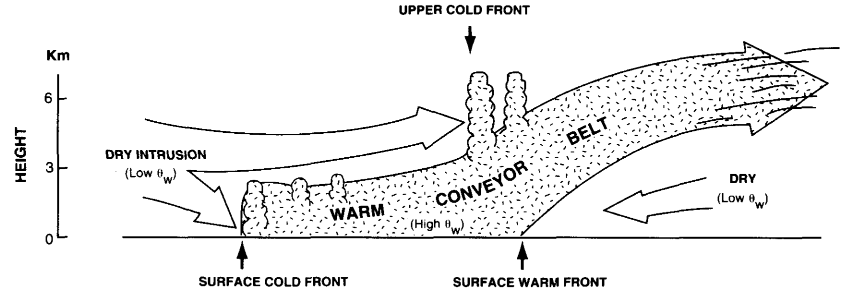

Fig. 1. Simple model of a kata-cold frontal situation in which dry air with low wet-bulb potential temperature (θ_w) overruns a shallow moist layer of high-θ_w air (Adapted from Browning, 1990). The present paper is concerned with the mesoscale structure of the surface cold frontal region.

an ana-cold front but on a much smaller scale. Both circulations are confined to the lowest 2.5 km of the atmosphere and can be thought of almost as boundary layer phenomena. In the case studied, the cold air was travelling over a relatively warm sea surface and the boundary layer was convectively unstable. We believe that our conceptual model may have implications for representing the mixing processes between such a convectively unstable boundary layer and the overlying free troposphere.

2. Context of the case study

The principal data used in this study are a sequence of dropwindsondes (hereafter referred to simply as dropsondes or sondes) released by the Meteorological Research Flight C-130 aircraft in the vicinity of a frontal cyclone during the FRONTS 92 experiment. The experiment was undertaken over the open sea (NE Atlantic) and presented an opportunity to study frontal structure in the absence of the complicating effects of topography. The broad features of the 27 April case presented in this paper have been described by Browning et al. (1995) and the basic data are given in Hewson (1993). Here we shall carry out a more detailed analysis of a small portion of the data, concentrating on part of a transect through a kata-cold frontal system that displayed two main SCFs. The criterion used by forecasters to classify a cold front as a kata-front is that the wind component (u) normal to the front should increase with height in the warm air. Fig. 2, depicting the vertical profile of u is consistent with this criterion.

Visible and infra-red satellite images for 1730 UTC on 27 April are shown in Figs. 3a, b, and the corresponding surface analysis is shown in Fig. 3c. The line AB in Fig. 3b is the aircraft track, relative to the frontal system, during the period from 1618 (at location A on the cold side) to 1742 (at the location B on the warm side of the frontal zone).

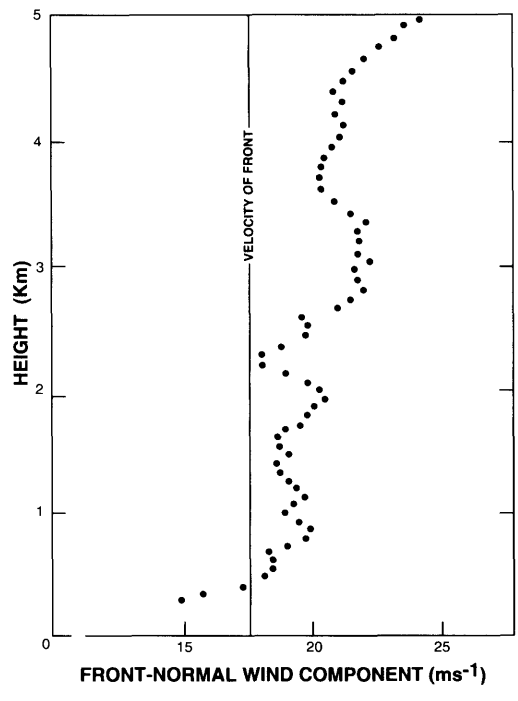

Fig. 2. Vertical profile of front-normal wind component (u) from sounding number 17 at location B in Fig. 3.

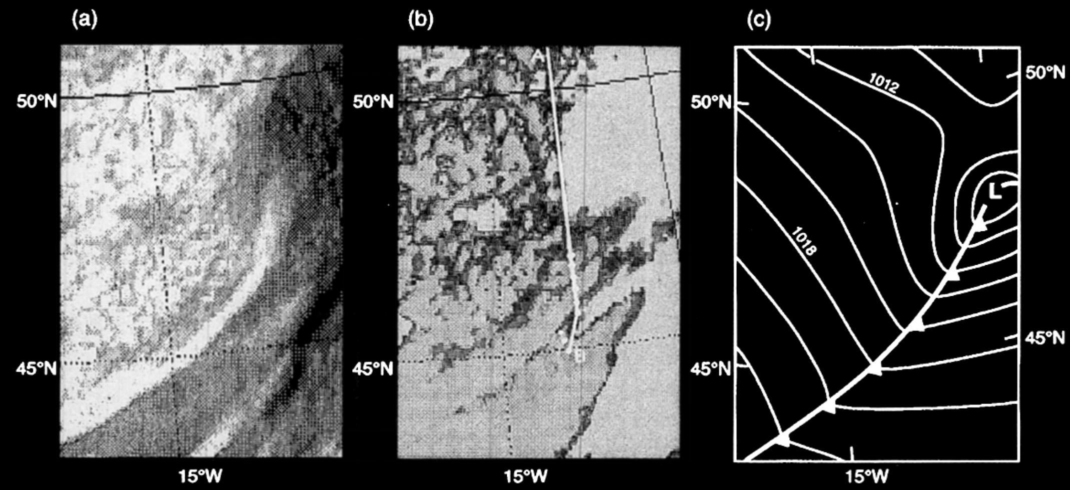

Fig. 3. (a) and (b) Meteosat imagery showing cold frontal cloud bands at 1730 UTC, 27 April 1992: (a) visible; (b) infra-red. The grey scale in (b) is enhanced to reveal fine structure in the low cloud region (tops with temperatures between +5°C and −3°C). AB is the track of the dropsonde aircraft; the nine dots at or near the southern end of the line are Sounding Numbers 11 to 19, as plotted in Figs. 5, 8. (c) Surface analysis for the area corresponding to (a) and (b) at 1800 UTC, 27 April. The frontal analysis is simplified and shows only SCF 1. (After Hewson, 1993).

Between A and B the aircraft track took it over shallow SCF cloud bands orientated SW–NE. Seventeen dropsondes were released between A and B, and the resulting pattern of relative humidity is shown in Fig. 4.

Cold, very dry, air (10 to 20% relative humidity above 3 km) was advancing over a relatively warm ocean. The resulting convectively unstable boundary layer showed considerable variation in structure associated with the SCF cloud bands. One feature to note in Fig. 4 is the way in which dry fingers penetrated slantwise to quite low levels (along the dashed axes in Fig. 4). Browning et al. (1995) show that the more well-defined fingers were laterally extensive and corresponded to laminae that were related to the banded cloud structures seen in the imagery. They present evidence from water vapour imagery to show that the dry laminae were associated with two rather larger-scale intrusions of dry air, the effects of which were felt at the surface as two cold fronts, labelled SCF 1 and SCF 2 in Fig. 4. We shall restrict our attention to SCF 1, especially the small rectangular inset drawn in Fig. 4. The associated cloud band as determined from satellite imagery is labelled C1 in Fig. 4.

3. Detailed mesoscale structure associated with SCF 1

3.1. The slantwise circulation

Near SCF 1, within the small region shown framed in Fig. 4, there were as many as 7 dropsondes, plus two more, slightly to one side of the section. Locations of all 9 sondes are shown by dots in Fig. 3b. The 3 northernmost sondes (numbered 11, 12 and 13 in Fig. 4) were above low cloud (tops at 1 km). The 5 southernmost sondes (numbered 15 to 19) were close to the cloud band associated with SCF 1, the tops of which extended up to about 2.4 km. In between, Sonde Number 14 fell through a cloud-free zone. This cloud-free zone shows up clearly as a dark strip in the visible imagery (Fig. 3a).

The detailed dropsonde analysis for SCF 1, based on the above 9 sondes, is shown in Fig. 5. Data have been plotted at height intervals of 80 m, each value being a running average over about 500 m (strictly 50 mb). Figs. 5a, b show aspects of the thermodynamic structure; shaded regions draw attention to regions of moist air (RH > 90%) and high θ_w (> 11°C), respectively. Fig. 5c shows the transverse wind component (u),

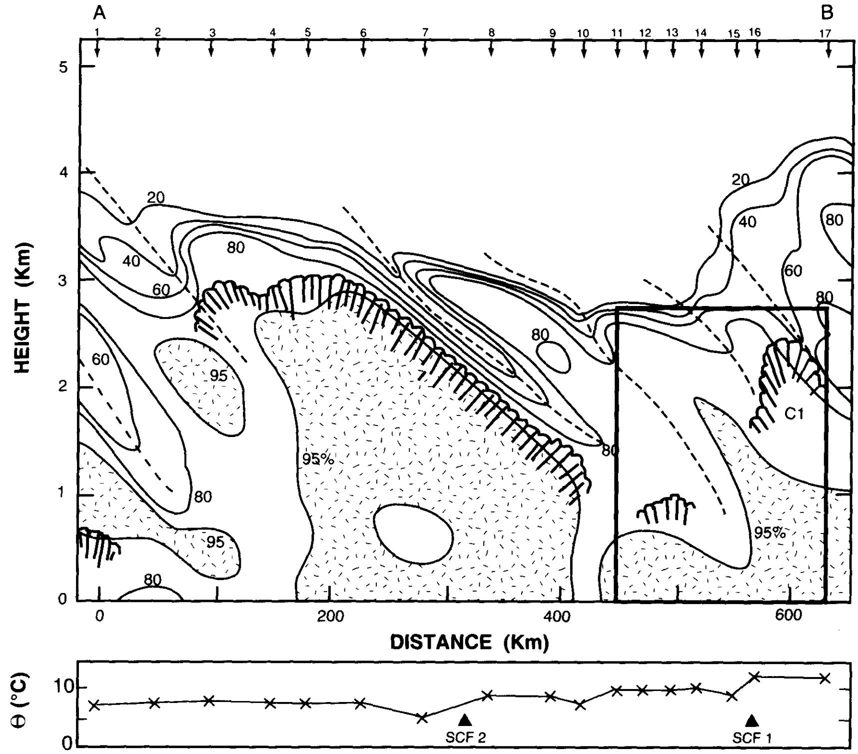

Fig. 4. Cross-section along AB (see Fig. 3b) showing isopleths of relative humidity superimposed upon outline of cloud tops derived from infra-red imagery. (After Browning et al., 1995). Locations of Soundings 1–17 are identified at top of diagram. Most of this paper is concerned with the detailed analysis of SCF 1 within the framed (bottom right) part of the diagram. The corresponding near-surface values of potential temperature (θ) are plotted in the panel at the foot of the diagram.

the shaded region corresponding to a minimum in u; the front itself was propagating with a u-component of between 17 and 18 m s^{-1} so that the shaded region was evidently a rearward-directed flow of up to 1 m s^{-1} relative to the front. We are attributing significance to quite small features in the analysed fields. We have confidence in the validity of such details because corresponding features can be clearly identified within sequences of sondes both in the thermodynamic fields and in the kinematic fields. As discussed in Browning et al. (1995), the accuracy of the winds was generally at least as good as 1 m s^{-1}; the consistency of the patterns in Fig. 5 suggests that the accuracy of the winds was even better than this.

In order to clarify the inter-relationship between the various fields, the isopleths bounding each of the shaded regions in Fig. 5 are plotted together in Fig. 5d. What emerges is a picture of a moist lamina associated with a rearward-directed flow of air with a θ_w of 11°C. Taking into account the fact that the section AB was not normal to the cold frontal bands (Fig. 3b), the moist lamina is estimated to have been inclined at roughly 1 in 40. This is consistent with rearward-sloping ascent within it of about 2 cm s^{-1}. Although the relative humidity in the moist lamina was high, it was generally subsaturated; indeed, except within about 10 km of the surface front, this was the very region that was cloud-free in the imagery.

3.2. The vertical convection

The satellite-detected cloud band associated with CF1 was situated mainly in advance of the

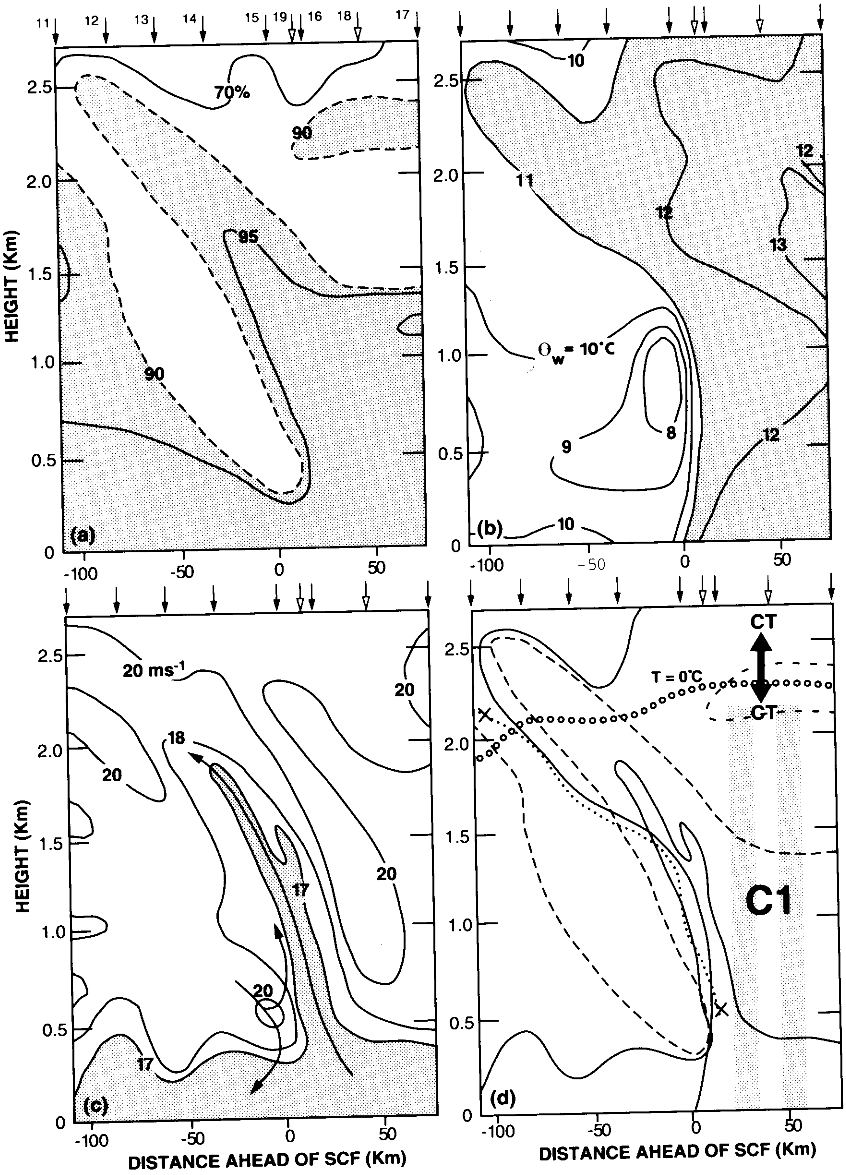

Fig. 5. Cross-section through SCF 1 along southern part of AB (see Figs. 3, 4), based on sounding numbers 11 to 19 (see arrows at top of diagram). The 4 panels show: (a) relative humidity (isopleths at 70, 90 and 95%, shaded above 90%), (b) wet-bulb potential temperature, θ_w (isopleths at 1°C intervals, shaded above 11°C, (c) front-normal wind component, u, (isopleths at 17, 18 and 20 m s^{-1}, shaded below 17 m s^{-1}; velocity of front is between 17 and 18 m s^{-1}). (d) superposition of isopleths from (a), (b) and (c), the isopleths shown being those that bound the shaded regions in (a), (b) and (c). Also shown in (d) are the $T = 0$°C isotherm (line of circles), the axis of maximum vertical shear of the front-parallel wind component, dv/dz (dotted curve labelled XX), and the region of convective cloud C1 (shaded), the arrow labelled CT-CT giving an indication of uncertainty in the cloud-top height.

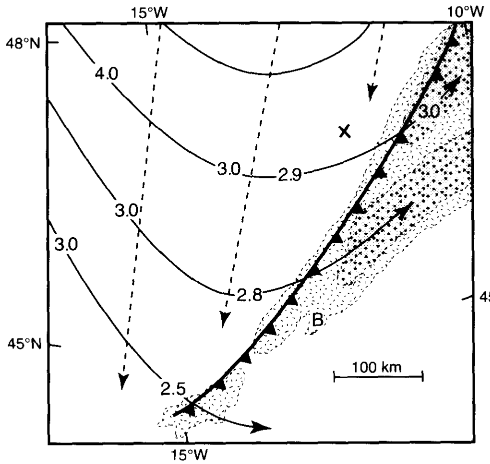

Fig. 6. Flow relative to SCF 1 in the 10°C and 25°C isentropic surfaces (dashed and solid lines, respectively). The 10°C flow descends from 1 km to the surface. Numbers along the 25°C streamlines give height of the 25°C surface in km. Cloud associated with SCF 1 is also shown (low cloud is stippled; slightly higher cloud with tops to 2.4 km is heavily stippled). XB marks the end points of the section in Fig. 5.

position of the surface cold front. As sketched in Fig. 5d, this cloud had tops up to 2.4 km $\pm$ 0.2 km, at which level the dropsondes showed a layer of air with $\theta_w = 12$°C that was characterised by slightly increased relative humidity. Fig. 5b shows that this is consistent with the convective ascent of air parcels from near the surface to their convective equilibrium level. Once they reached this level, Fig. 5c shows that they will have entered a region where the flow was overtaking the front at about 2 m s^{-1}. In fact there were also strong components of flow perpendicular to the plane of Fig. 5 which we can examine via an analysis in plan view (Fig. 6).

Fig. 6 shows a tracing of the cloud band associated with CF1, derived from the infra-red imagery (Fig. 3b). The heavily stippled regions show deeper cloud (tops to about 2.4 km) embedded within a broader region of shallower cloud (lightly stippled). As often happens, the convective cloud tops extend downwind at an angle (about 20°) to the overall frontal cloudband. Parts of the isentropic analyses for the $\theta = 10$°C surfaces, derived by Browning et al. (1995), are superimposed on the satellite-derived cloud pattern in Fig. 6. These show that the relative flow in the 10°C θ-surface just behind SCF 1 descended from the north and terminated behind the surface front. However, the relative flow in the 25°C surface descended toward the front from the northwest, and then veered, before crossing over the front just above the cloud tops and ascending toward the northeast. The flow at the level of the cloud tops behaved similarly. The convective cloud tops were aligned with this flow.

3.3. *Vertical mixing associated with the circulations*

A simplified interpretation of Fig. 5, depicting the nature of the slantwise and vertical circula-

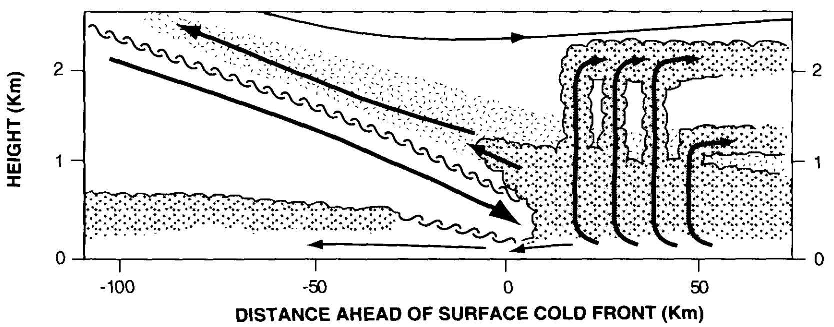

Fig. 7. Conceptual model of circulations at the surface cold front (SCF). Based on Figs. 5, 8 but stretched 4-fold to provide a rather more realistic aspect ratio. Cloudy boundary layer and ex-boundary-layer air is stippled heavily. Vertical arrows ahead of the SCF represent convection. Inclined arrows behind the SCF represent slantwise ascent and descent on either side of a strongly sheared layer with low Richardson Number depicted by the wavy line. The lightly stippled layer, above the wavy line represents a moist but unsaturated layer originating from just above the boundary layer.

tions, is shown in Fig. 7. The vertical arrows represent upright convection lifting air from close to the surface to 2.4 km just ahead of the SCF. The two bold inclined arrows represent the slantwise circulation, and the wavy line in between represents a shear zone. Fig. 8 shows that this shear zone was associated with a coherent layer of low Richardson Number (Ri). Measured over 500 m (strictly 50 mb) layers, the minimum values of Ri were slightly less than 1. Coherent patterns were still achieved when Ri was evaluated over even shallower, 200 m layers (strictly 20 mb): within the dashed isopleths in Fig. 8 the resulting Ri fell below the critical value of 0.25 for Kelvin-Helmholtz instability.

Clearly the convective cells were effective in mixing boundary-layer air up to 2.4 km (and

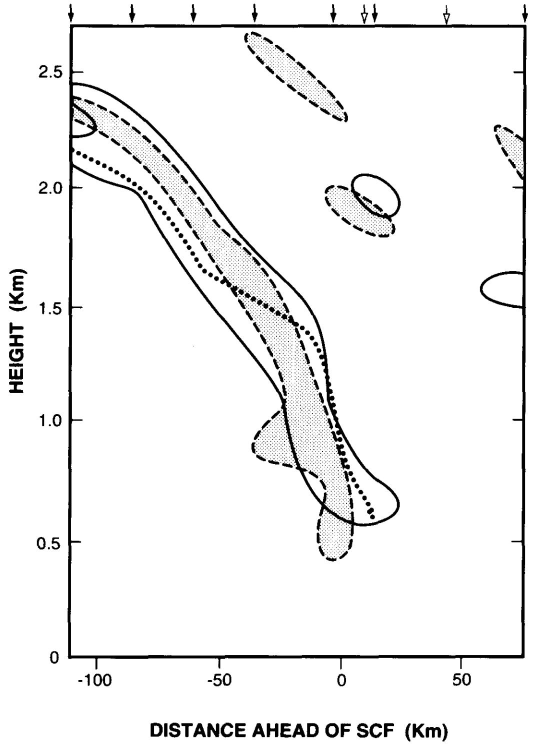

Fig. 8. Cross-section through SCF 1 as in Fig. 5 but showing Richardson Number. The solid isopleth encloses regions where $Ri < 1.0$ measured over 50 mb layers. The dashed isopleth encloses stippled regions where $Ri < 0.25$ measured over 20 mb layers. The dotted line, taken from Fig. 5d, is the axis of maximum dv/dz.

higher in parts of the front closer to the cyclone centre). What is not so clear is the role played by the shear layer in mixing boundary-layer air into the free atmosphere. One's first impression is of the ascending branch of the slantwise circulation lofting boundary-layer air into the free atmosphere. The fact that much of this flow (lightly stippled area in Fig. 8), though close to saturation, was cloud-free suggests instead that the air within it originated from just above the boundary layer. Alternatively, it might have consisted of some boundary-layer air that was being diluted through mixing with dry air from the descending limb of the slantwise circulation. A close comparison of Fig. 8 with Fig. 5c, however, shows that the layer with $Ri < 0.25$, though contiguous with, does not overlap with, the core of the rearward-directed flow, and so it appears unlikely that this mixing could account for the sub-saturation of the entire slantwise ascending flow.

We thus obtain a picture of a slantwise circulation in the form of a thinly laminated shear layer (vortex sheet) perturbing the top of the boundary layer. According to Browning et al. (1995), the best-defined of such vortex-sheets correspond to the leading edges of fresh injections of dry-intrusion air descending from upper levels, as seen in satellite water vapour imagery. The descending part of the slantwise circulation intrudes into the boundary layer and partially mixes dry air down to the surface just behind the SCF. The mixing is depicted schematically in Fig. 7 by the wavy line (representing Kelvin-Helmholtz billows). Very close to the surface there is a fritionally-induced flow of moist boundary-layer air rearwards relative to the advancing front, but this flow mixes with the descending dry air, leading to the well-defined clearance of the cloud. Meanwhile the region of slantwise ascent lifts and pulls out a layer of air from the top of the boundary layer just ahead of the SCF. The region of slantwise ascent also starts to lift and pull out air from within the boundary layer but, at least in the present case, this realizes the potential instability and triggers shallow vertical convection. As a result, boundary-layer air that otherwise would have ascended within the slantwise circulation or perhaps remained within the boundary layer, convects vertically to a level where the flow is overtaking the front. At this level the cloudy air is detrained and may eventually create a new (higher) boundary layer top.

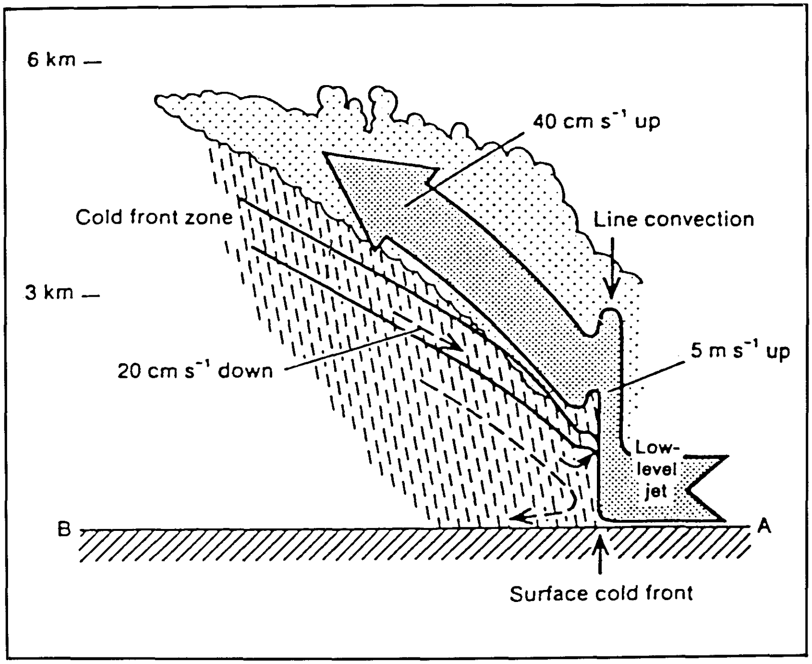

Fig. 9. Simple model of the airflow at an ana-cold front showing warm conveyor belt air with high θ_w (bold arrow) originating at low levels ahead of the front and undergoing rearward-sloping ascent above descending air within the cold frontal zone (Browning, 1990).

4. Concluding remarks on some similarities in the structure of kata- and ana-cold fronts

In the introduction, we described kata-cold fronts as being *superficially* different from ana-cold fronts. Certainly this author (Browning, 1990) has represented them as two poles in a frontal classification scheme. This is still a valid perspective when viewing the fronts in terms of their broad-scale behaviour: thus the conceptual model of an ana-cold front in Fig. 9 is clearly quite different from the model of a kata-cold front in Fig. 1. However, we have shown in this paper that, when a kata-cold front is viewed on the mesoscale, it may be seen to have embedded within it the rudiments of a rearward-sloping circulation (Fig. 7).

In an ana-cold front the boundary-layer air is to a large extent peeled off into a strip of forced line convection before ascending slantwise to the rear. As a result of the wholesale peeling off of boundary-layer air, there is an abrupt drop in surface temperature at such a front. In a kata-front the surface temperature drop tends to be smaller since only some of the boundary-layer air is vented out of the boundary layer, and only a small fraction of this may undergo rearward slantwise ascent. Yet the elements of an ana-cold frontal slantwise circulation may still be there. Evidently, therefore, it is not a discontinuous step for one kind of frontal circulation (kata) to evolve into another (ana): it is merely a matter of the slantwise circulation becoming quantitatively more intense and larger. Future observational studies might reveal that satellite-detected "cloud heads" evolve in this way.

The conceptual model in Fig. 7 implies rather specific but complicated coupling of processes leading to vertical fluxes through the boundary layer in the vicinity of the surface front. Detailed studies using a cloud-resolving model need to be undertaken in order to understand these processes so that they may eventually be parameterized within larger scale models.

5. Acknowledgements

I am grateful to Clare Davitt for providing the dropsonde data and to the team led by Sid Clough who ran the FRONTS 92 experiment. The Joint Centre for Mesoscale Meteorology is supported by the Meteorological Office and the Department of Meteorology, University of Reading.

REFERENCES

Bergeron, T. 1937. On the physics of fronts. *Bull. Amer. Meteorol. Soc.* **18**, 265–275.

Browning, K. A. 1990. Organization of clouds and precipitation in extratropical cyclones. In: *Extratropical cyclones: the Erik Palmén Memorial Volume*, C. W. Newton and E. O. Holopainen, eds. American Meteorological Society, 129–153.

Browning, K. A., Clough, S. A., Davitt, C. S. A., Roberts, N. M., Hewson, T. D. and Healey, P. G. W. 1995. Observations of the mesoscale sub-structure in the cold air of a developing frontal cyclone. *Quart. J. Roy. Meteor. Soc.* **121**, in press (July 1995 issue).

Browning, K. A. and Monk, G. A. 1982. A simple model for the synoptic analysis of cold fronts. *Quart. J. Roy. Meteor. Soc.* **108**, 435–452.

Hewson, T. D. 1993. The FRONTS 92 Experiment: A quick look atlas. *JCMM Internal Report no. 15.* 176 pp. Available from the National Meteorological Library and Archives, Meteorological Office, Bracknell.

Sansom, H. W. 1951. A study of cold fronts over the British Isles. *Quart. J. Roy. Meteor. Soc.* **77**, 96–120.

Printed in Belgium

NOTES TO CONTRIBUTORS

Tellus publishes articles, short contributions and correspondence. Authors submitting a contribution do so on the understanding that the work has been read and approved by all authors and that no similar paper, other than an abstract or preliminary report, has been or will be submitted for publication elsewhere. Short contributions should not exceed 4 printed pages. Correspondence is intended for discussion of papers published in TELLUS and should not exceed one printed page.

Copyright. The submission of a manuscript means that the authors agree to assign exclusive copyright to Munksgaard International Publishers if and when the manuscript is accepted for publication. The work must not be published elsewhere in any language without the written consent of the TELLUS Editorial Office. Articles published in TELLUS are protected by copyright, which covers translation rights and the exclusive right to reproduce and distribute all of the articles printed in TELLUS. No material published in TELLUS may be stored on microfilm or videocassettes or in electronic databases and the like without the written permission of TELLUS. However, TELLUS does not require that permission be obtained from the Editorial Office for the use of *tables* and *figures* published in TELLUS, provided that the source be appropriately cited.

Manuscripts. The manuscript should be typed on one side of the page with wide margins and double-spacing. All pages should be consecutively numbered. Mathematical work should be carefully written leaving a wide space above and below each character for remarks for the printer.

Manuscripts (4 copies) should be sent to:

TELLUS
Editorial Office
Arrhenius Laboratory
S-106 91 Stockholm
Sweden

Illustrations. Originals or glossy prints of drawings should be about twice the final size (width: max 28 cm, min 14 cm; height: max 34 cm) with lettering large enough to remain clearly legible when reduced. Maps should preferably be oriented so that the meridian through the center of the drawing is parallel to the sides. Figure legends should be self-explanatory and typed on a separate sheet of paper. They should also be typed below each figure on all copies. All figures should be numbered consecutively and mentioned specifically in the text by number. The number and orientation should be noted on the back of each figure as well as the name(s) of the author(s). Originals should not be sent until the paper has been accepted.

Units, abbreviations and symbols. The "Système International d'Unités" (SI units) should be used. However, the units hPa and mb are accepted. Only standardized terms which have been generally accepted should be used. Unfamiliar abbreviations must be defined when first used. Particular care should be taken to ensure that all symbols are clearly identified.

Abstract. An abstract should be provided.

References. Articles should be fully documented with references in the text and reference listings grouped alphabetically by authors' names at the end of the paper. The order for references to articles is: author(s), year, title of article, abbreviated title of journal (italics), volume number (bold), first and last pages; and for articles in book form: author(s), year, title of article, title of book (italics), editor(s) (in brackets), publisher, city of publication, first and last pages. Titles of journals should be abbreviated according to *International list of periodical title word abbreviations* (International Standard 833-ISO). References to unpublished manuscripts or manuscripts in the submitted stage cannot be allowed.

Examples:

Raustein, E., Sundqvist, H. and Katsaros, K. B. 1991. Quantitative comparison between simulated cloudiness and clouds objectively derived from satellite data. *Tellus* **43A**, 306–320.

Schell, D. and Georgii, H.-W. 1989. Design and operation of a two-stage fogwater collector. In: *Mechanisms and effects of pollutant-transfer into forests* (ed. H.-W. Georgii). Kluwer Academic Publishers, Dordrecht, 221–229.

Proofs. Copies of the proofs together with the manuscript will be sent to the author. One corrected proof and the manuscript should be returned to the publisher without delay. Excessive changes made by the author in the proofs, excluding printer's errors, will be charged to him separately.

Page Charges. The first 5 pages of an article will be published free of charge. Additional pages are subject to a page charge on the following scale: up to 5 excess pages, USD 70 per page; following excess pages, USD 120 per page. (For special issues, other conditions for page charges may be agreed.) *Invoices for page charges will be sent from the Editorial Office in Stockholm.*

Offprints. Authors of articles receive 50 offprints free of charge. Additional offprints must be paid for by the author. These will be charged in *Danish kroner* by MUNKSGAARD. Request forms for offprints will be sent out with the proofs.